Decarbonization of the Cargo Shipping Fleet

Decarbonization of the Cargo Shipping Fleet

Julie Chalfant (M)[1], Hauke Kite-Powell (M)[2], Luca Bonfiglio (M)[1], Chryssostomos Chryssostomidis (LF)[1]
1. Sea Grant Design Laboratory, Massachusetts Institute of Technology, Cambridge, Massachusetts 02139
2. Marsoft, Inc., Boston, Massachusetts 02109

In an effort to combat climate change, the International Maritime Organization (IMO) has set ambitious goals for the reduction of greenhouse gas emissions from ships, with a target of at least a 50% reduction of total annual greenhouse gas (GHG) emissions, including carbon, from 2008 levels by 2050, with a further goal of zero GHG emissions within this century. Numerous technologies are under development to address these new goals, but the implementation of these new technologies is quite uncertain. Cargo ship owners face the challenge of determining how to best employ and possibly upgrade the current fleet to meet interim goals while awaiting the maturation of future technologies. This paper describes a methodology and computer code that provide a rapid assessment of the impact of various fuel-saving technologies on an existing cargo ship's fuel consumption, thus providing the ship owner fundamental data indicating which upgrades and practices warrant further, more detailed investigation.

KEY WORDS: Decarbonization; Cargo Shipping; Ship Design

BACKGROUND

According to the National Oceanic and Atmospheric Administration, the amount of carbon dioxide in the atmosphere has increased by 1.78 ppm per year on average since 1980, and the increase is accelerating. Through the 1980s and 1990s, the increase was around 1.5-1.6 ppm per year, but the growth rate has averaged 2.4 ppm per year since 2010 (Tans et al. 2020).

Rising levels of carbon dioxide in the atmosphere adversely impact the environment in many ways. For example, increased levels of carbon dioxide dissolving in sea water increase the acidity of the oceans; as pH levels drop, organisms like oysters and corals have trouble maintaining their hard shells and skeletons made from calcium carbonate. If pH levels get too low, the calcium carbonate structures begin dissolving (NOAA 2020). Another example can be found in the NOAA Arctic Report Card which each year shows an Arctic that is becoming warmer, less frozen and more fragile; the 2020 report includes data on high land-surface air temperatures, low snow extent, low minimum sea-ice extent, and extreme wildfires (Thoman et al. 2020).

Shipping is the most carbon-efficient method of transporting cargo per tonne-km of cargo moved; a very large crude carrier (VLCC) ship emits 3 grams of carbon per tonne-km of cargo, compared to 80 for a 40-tonne truck and 435 for a 747 aircraft (Buhaug et al. 2009). However, the efficiency of cargo shipping is juxtaposed against the sheer quantity of goods transported by ship over vast distances; per the UN Review of Marine Transport (UNCTAD 2018), approximately 80% of world trade by volume, and 70% by value, is carried by ship. This results in cargo shipping contributing between 2 and 3% of total worldwide carbon emissions per year.

In an effort to combat climate change, the International Maritime Organization (IMO) has set ambitious goals for the reduction of greenhouse gas emissions from ships, with a target of at least a 50% reduction of total annual greenhouse gas (GHG) emissions, including carbon, from 2008 levels, by 2050 (International Maritime Organization 2020). Numerous interim goals step the cargo fleet toward the 50% by 2050 target.

Achieving these goals will require the combination of a large variety of actions and technology advancements; there is no silver bullet that will achieve the targeted reductions alone. Long-term possibilities such as the development and shipboard implementation of new fuels, renewable energy, and energy storage will have a huge impact on shipboard CO2 production, but there is great uncertainty about which of these technologies will become the best option for both the earth and the shipping companies.

While the research and development required to bring these new technologies to fruition is being accomplished, numerous actions can be taken immediately to reduce the carbon production and extend the useful life of currently existing ships within the new GHG requirements, thus allowing ship owners time to assess new technologies before committing to new-construction vessels that incorporate them.

INTRODUCTION

An easy-to-use computer code was constructed that provides ship owners fundamental data indicating which technologies and practices are likely to have a significant impact on the owner's fleet by providing an assessment of the impact of various fuel-saving technologies on a specific cargo ship's fuel consumption. These fuel-saving technologies and practices include slow steaming, engine modifications, bulbous bow removal, propeller optimization, and energy-saving devices that modify the hull. For each modification or combination of modifications, the code provides quantified impact in terms of specific fuel consumption and fuel usage in tonnes per day for a given loading condition of a given ship.

The computer code created through this project accomplishes a rapid assessment of a ship's performance using a small amount of data. The code is designed to be easy to use, depending on ship data that is readily available to the ship owner.

The code calculates the ship resistance over a range of speeds, estimates propeller performance, and predicts engine performance, all at design draft. If ballast draft information is provided, similar calculations are accomplished at ballast condition as well. The code also estimates ship performance with the bulbous bow removed, with an energy saving device installed, with various engine modifications implemented, or with a modified propeller designed for a different design speed, and with combinations of these modifications. The primary metric for comparison is fuel consumption.

The EPA recommends a common conversion factor of 10.21 kg of CO2 emissions per gallon of diesel fuel consumed (U.S. Environmental Protection Agency 2020). Diesel 4, typically used in slow-speed engines, has a density of 959 kg/m^3 (Engineering Toolbox 2022) or approximately 3.63 kg per gallon of fuel. Thus, approximately three tons of carbon dioxide emissions are saved for every ton of fuel saved.

This article provides an overview of the code structure and input data, describes the theoretical background supporting hull, propeller and engine calculations, describes the methodology for assessing the impact of ship modifications on fuel consumption, addresses the calculations and estimates required to flesh out the data set, uses the code to analyze various ship types and compares the results to actual ship performance, and provides conclusions and recommendations for future work.

CODE OVERVIEW

Following is an overview of the program structure. Theoretical underpinnings of each segment can be found in the subsequent sections. The original concept of the code is based on work by Bonfiglio and Boote (2009).

Data Input

Input data are provided by the user in an Excel file. The minimum data required include ship type, length, beam, draft, displacement, design speed, number of propellers, engine layout data, and indication of the presence of a bulbous bow or energy-saving device; see Table 1. The accuracy of resistance estimates can be improved by increasing the amount of data provided to the program including information such as bulbous bow dimensions, longitudinal center of buoyancy, hull shape coefficients, surface areas, and propeller details. If these additional data are not provided, the program estimates input values.

Table 1. Minimum required input data.

Displacement or Deadweight
Length
Beam
Draft
Design Speed
Number of Propellers
Ship Type Indicator (Tanker, Container)
Bulbous Bow Indicator (yes, no)
ESD Indicator (yes, no)
Engine Layout Diagram including for each corner:
Rotation Rate
Brake Power
Mean Effective Pressure
Specific Fuel Oil Consumption

Since hullform and propeller models of sufficient detail to accomplish a full computational fluid dynamics (CFD) analysis of a hull are not typically available, various standard estimation methodologies for ship and propeller performance are used instead.

Incorporated into the program is a library of engines, including a wide range of MAN B&W and Wärtsilä marine diesel engines plus a few from other manufacturers. The library is stored in an Excel spreadsheet, to which the user may add new engines if desired. This library was compiled from data catalogs available from the manufacturers, e.g. MAN Energy Solutions (2018).

During the data input period, the program reads and parses the input data, estimates missing data as appropriate, and sets constants.

As-Built Ship Calculations

For each ship in the input database, the following calculations are conducted at design draft. If ballast draft information is provided, then the same hull, propeller and engine combination that was used in the design draft calculations is analyzed at ballast draft.

Calculations at Design Draft

Ship Resistance is calculated at design draft using the Holtrop and Mennen procedure for tankers and bulkers or the Hollenbach procedure for container ships, producing

curves of resistance and effective power over a range of speeds. Resistance estimates include frictional resistance, form factor, appendage resistance, wave resistance, bulbous bow impact, air resistance, and correlation allowance.

Propeller Performance is calculated using the Wageningen B-Series propeller regression formulas and the input data. If expanded area ratio (AE/AO) or pitch to diameter ratio (P/D) are not provided by the user, then the program designs a propeller that produces the lowest fuel oil consumption at design speed when coupled with the given engine, while limiting cavitation. Once AE/AO and P/D are set, the program calculates propeller efficiency, estimates hull efficiency and relative rotative efficiency, and uses the input shaft efficiency to calculate delivered and brake power over a range of speeds.

Engine Performance. The engine design operating point, termed specified maximum continuous rating (SMCR), is calculated using the brake power and rotation rate of the propeller at the design speed. Fuel oil consumption is calculated over the full range of speeds supported by the engine, assuming tuning at the SMCR point.

Calculations at Ballast Draft

Ship Resistance is calculated at ballast draft, producing curves of resistance and effective power over a range of speeds at the appropriate draft.

Propeller Performance. The propeller curves determined at design draft are used to calculate propeller performance at ballast draft, providing estimates of delivered and brake power over a range of speeds.

Engine Performance. Using the SMCR point calculated at design draft, fuel oil consumption is calculated at ballast draft over the full range of speeds supported by the engine.

Performance Improvements

The following performance improvements can be calculated individually or in combinations. It is possible to combine any of these major modifications with any other, with the exception that only one engine modification can be selected at a time. Note that the impacts of combinations of improvements are not linear, so to calculate the overall impact, one must accomplish the analysis with multiple improvements selected, rather than summing the results of various individual improvements.

Engine Modifications. Estimates of fuel oil consumption for a variety of engine modifications appropriate to the installed engine are provided over the range of speeds available.

Propeller Optimization. The propeller may be redesigned for a slower design speed by removing the AE/AO and P/D from the input data and designating a new design speed and maximum speed for cavitation purposes.

Bulbous Bow Removal. If a bulbous bow is present, estimates for the impact of removing the bulbous bow are provided by reducing hull wetted surface area by the surface area of the bulb, and eliminating the bulbous bow impact in the resistance calculation.

Energy Saving Device Addition. The impact of adding an energy saving device is estimated through an added efficiency value.

Output Data

Output from the program is provided in numerical tables and in graphical format. Resistance data, propeller data, and fuel usage are provided along with tabulation of input and calculated values for all variables.

User's Guide

Further description of the code along with examples are provided in the remainder of the article. A very thorough theoretical background and a user's guide are available in (Chalfant et al. 2021).

RESISTANCE CALCULATION

Holtrop and Mennen

Ship resistance for tankers and bulkers is estimated from basic hullform characteristics using the method developed by Holtrop and Mennen (1978, 1982) and Holtrop (1984, 1988). This method predicts full-scale ship resistance through a regression analysis of many towing-tank resistance model tests of various hullforms. The methodology estimates wave resistance, frictional resistance modified by a form factor, air resistance, a correction factor for roughness and ship form, and the resistance impacts of appendages and bulbous bow as applicable; these are combined to predict ship resistance in calm water with no wind, referred to herein as ship resistance at trial condition, or R_{TC}. Figure 1 shows the calculated resistance data for an example ship.

The description of Holtrop and Mennen's method as described in Birk (2019) is followed herein. Total resistance at trial condition, R_{TC}, is the total resistance in calm, deep water with no wind,

$$R_{TC} = R_f(1+k) + R_{app} + R_w + R_a + R_{aa}. \qquad (1)$$

R_f is frictional resistance calculated using the ITTC-57 correlation line; this value is modified by a form factor, $(1+k)$, which accounts for differences between the ship's form and a flat plate. R_{app} is appendage resistance, calculated using the appendage surface area and a form factor based on the

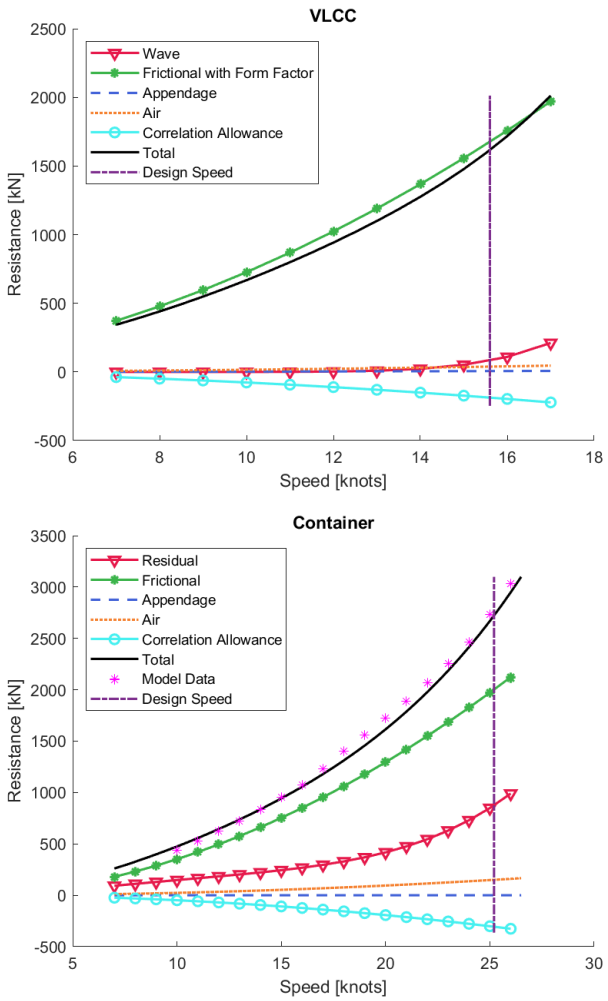

Fig. 1. Resistance calculated using the Holtrop and Mennen procedure for a VLCC (top) and using the Hollenbach procedure for a container ship (bottom).

type of appendage. R_w is wave resistance, calculated using a regression analysis of tow tank data, provided as a function of Froude number. R_a is change in resistance due to the correlation allowance, discussed below. R_{aa} is air resistance, based on the transverse cross-sectional area of the ship above the waterline including deckhouse and loaded cargo. Holtrop and Mennen's original research included values for transom resistance and change in pressure due to the bulbous bow, but subsequent research indicates that both values should be omitted.

Bulbous Bow Impact. Holtrop and Mennen account for the impact of the bulbous bow by applying a correction, c_2, to the wave resistance, thus reducing wave resistance when a bulbous bow is present. They suggest

$$c_2 = e^{-1.89\sqrt{c_3}} \tag{2}$$

in which

$$c_3 = \frac{0.56 A_{bt}^{1.5}}{BT(0.31\sqrt{A_{bt}} + T_f - h_b)}, \tag{3}$$

where A_{bt} is the transverse cross-sectional area of the bulb at the forward perpendicular, h_b is the height of the centroid of that area above baseline, and T_f is the draft at the forward perpendicular. This equation applies a reduction in wave resistance due to the bulbous bow; the reduction is a constant percentage of the wave resistance.

The frictional resistance impact of the bulb is inherently included in the whole ship frictional resistance calculation since the ship wetted surface area includes the surface area of the bulb.

Note that the only characteristics of the bulb that are used in this calculation pertain to the area and centroid of the transverse cross-section of the bulb at the forward perpendicular; this is a small set of data to capture an extremely widely varying set of possible shapes and impacts of a bulbous bow, and is thus a very rough approximation of the impact of the bulb on the performance of the ship. Further discussion of various bulbous bow estimation methodologies can be found in (Chalfant et al. 2021).

Correlation Allowance. A correlation allowance accounts for differences between model and full scale results for effects such as roughness allowance and the partial dynamic similarity of the model test. While correlation allowances have historically been assigned a constant value of 0.0004, it has been found more recently that the correlation allowance should be varied with size of the vessel. A variety of correlation allowances are proposed by different authors; an estimate from Kristensen and Lützen (2012) is used

$$C_a = \left(\frac{log_{10}\Delta}{2} - 0.1(log_{10}\Delta)^2\right)/1000 \tag{4}$$

where Δ is the ship displacement in metric tonnes. A lower limit of -0.0001 is placed on C_a. The correlation allowance resistance adjustment, R_a, is

$$R_a = \frac{1}{2}\rho V^2 C_a\Big(A_{ws} + A_{app}\Big), \tag{5}$$

where ρ is the density of seawater, V is the ship speed through the water, A_{ws} is the wetted surface area of the bare hull, and A_{app} is the total wetted surface area of all appendages. Note that the correlation allowance can be negative, in which case it reduces the total calculated ship resistance.

Hollenbach

Ship resistance for container ships is estimated using the method developed by Hollenbach, who performed a regression analysis of tow tank data taken in Vienna, Austria. Hollenbach provides a mean estimate of resistance along with an upper and lower bound. Only the mean value is used herein. Hollenbach's method provides separate analyses for design draft and ballast condition.

The description of the method provided by Birk (2019) is followed. Total resistance at trial condition is

$$R_{TC} = R_f + R_r + R_{app} + R_a + R_{aa}. \tag{6}$$

R_f is frictional resistance calculated using the ITTC-57 formula, but without a form factor. R_r is residuary resistance, accounting for wave and form drag, which is calculated as a function of Froude number and block coefficient, with different regression coefficients available for single-screw ships at design draft and ballast draft and for twin-screw ships at design draft. The residuary resistance is modified by factors for length, beam-to-draft ratio, length-to-beam ratio, wetted length, aft overhang, trim, and propeller diameter, and, for twin-screw ships, the number of rudders, brackets, bossings and thrusters. Appendage resistance, R_{app}, and air resistance, R_{aa}, are calculated in the same manner as Holtrop and Mennen.

All calculations are performed using a calculation length, L_c, which is based on the overall length of the wetted surface area of the ship; thus, any impact of the bulbous bow is included purely through the length of the bulb forward of the forward perpendicular and the surface area of the bulb.

The bottom image in Fig. 1 shows the calculated resistance data for an example ship using Hollenbach.

PROPELLER CALCULATION

Propeller performance characteristics are estimated using the Wageningen B-series propeller data as described in (Lewis 1988). This regression analysis provides thrust coefficient, K_T, torque coefficient, K_Q, and open-water efficiency, η_o, as a function of advance ratio, J, based on the provided values of propeller diameter, D, number of blades, Z, pitch/diameter ratio, P/D, and expanded area ratio, AE/AO. Only fixed-pitch propellers with one propeller per shaft are addressed; counter-rotating propellers and controllable-pitch propellers are not treated.

Resistance Input to Propeller Calculation

Ship resistance versus speed is calculated using the method described the previous two sections of the article, producing "trial condition" resistance, R_{TC}, *i.e.* resistance in deep, calm water with no wind.

The "heavy running" resistance, R_{HR}, which includes the impact of wind and waves, is estimated by increasing the calm water resistance by a sea margin, sm, provided by the user;

$$R_{HR} = R_{TC}(1 + sm). \tag{7}$$

The sea margin can vary depending on the type of ship and the planned operational area, but a typical value is 15%; this is the value assumed if the user does not input a value.

If the ship is not at even keel, then the thrust from the propeller is not directly forward. Therefore, the thrust is increased by a trim factor

$$F_{trim} = \sqrt{1 - \left(\frac{|T_a - T_f|}{L_{bp}}\right)^2} \tag{8}$$

where T_a is draft at the aft perpendicular, T_f is the draft at the forward perpendicular, and L_{bp} is the ship length between perpendiculars. For a twin-screw ship, equal loading of the propellers is assumed, so the thrust for each propeller is one-half of the total thrust. Thus, the resistance value used in estimating propeller performance, R_T, is

$$R_T = \frac{R_{HR}}{F_{trim} N_p} \tag{9}$$

where N_p is the number of propellers.

Propeller Curves

It is assumed that the Wageningen B-Series propeller is indicative of the propeller used in the ship, and the performance characteristics of the propeller are calculated using the regression formula coefficients as described in (Lewis 1988). This has been found to be a good assumption in all cases for which propeller data was consulted.

The defining curves for propeller performance in open water are the non-dimensional thrust coefficient, K_T, and the non-dimensional torque coefficient, K_Q, both functions of the non-dimensional advance ratio of the propeller, J. The open water efficiency of the propeller is

$$\eta_o = \frac{JK_T}{2\pi K_Q}. \tag{10}$$

The K_T and K_Q curves are estimated using Wageningen's equations,

$$K_T = \sum C_{kt} Z^{zt} (AE/AO)^{at} (P/D)^{pt} J^{jt} \tag{11}$$

and

$$K_Q = \sum C_{kq} Z^{zq} (AE/AO)^{aq} (P/D)^{pq} J^{jq}, \tag{12}$$

where Z is the number of blades, AE/AO is the expanded area ratio, P/D is the pitch to diameter ratio, and C_{kt}, C_{kq}, zt, at, pt, jt, zq, aq, pq and jq are coefficients and terms of the Wageningen B-screw Series found in (Lewis 1988).

Propeller curves for a representative propeller are plotted versus J in Fig. 2.

If the number of blades is not provided by the user, four blades are assumed. If the pitch to diameter ratio is not provided, the P/D ratio that produces the best fuel oil consumption at design speed is chosen, using the methodology described in the section on propeller optimization below. If the expanded area ratio is not provided, the formulation proposed by Keller and reported in Birk (2019) is used in which

$$AE/AO = \frac{(1.3 + 0.3Z)T_o}{(p_o - p_v)D^2} + k \tag{13}$$

where Z is the number of blades, T_o is the thrust, $(p_o - p_v)$ is the pressure at the center of the propeller hub, and k is a constant that varies with the type of ship. The values $k = 0.2$ for single-screw vessels, $k = 0.1$ for high-speed twin-screw vessels (with design speeds greater than 20 knots), and $k = 0.0$ for slower twin-screw vessels are used. The Keller criteria selects an expanded area ratio that is likely to meet cavitation criteria. After calculating propeller performance, cavitation is estimated and AE/AO is adjusted if necessary as discussed in the section on cavitation below.

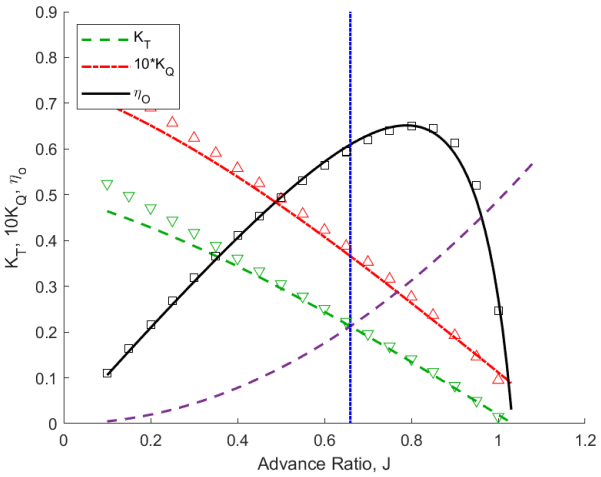

Fig. 2. Propeller curves. The propeller operating point (blue dotted line) at a given speed is determined by the intersection of the ship-specific K_T curve (purple dashed line) and the propeller-specific K_T curve (green dashed line). Note that estimates are extremely good in the area of interest, between J of 0.6 to 0.7, even for a container ship with a highly-skewed propeller. Propeller test data for the corresponding propeller are depicted with symbols.

Propeller Operating Point

To remove the dependence of the propeller curves on propeller rotation rate, which is unknown at this point, K_T is divided by J^2 such that

$$\frac{K_T}{J^2} = \frac{T_o}{\rho D^2 V_a^2}, \tag{14}$$

where T_o and V_a are calculated as described above, and D is provided by the user or estimated.

At any given speed and sea state, the intersection of the curve defined by Eq. 14 multiplied by J^2 (for the particulars of the ship), and the propeller K_T curve defined by Eq. 11 (for the particulars of the propeller), determines the J value at which the propeller will operate when installed in the given ship at the given speed and sea state; an example is shown in Fig. 2.

Once J is determined for a given operating point, the propeller rotation rate and open water propeller efficiency can be calculated at that speed and sea state using Eq. 10 along with the definition of J,

$$J = \frac{V_a}{nD}. \tag{15}$$

Curves of delivered power versus ship speed, propeller rotation rate versus ship speed, and propeller efficiency versus ship speed are produced for the trial condition and heavy running condition.

Cavitation

Cavitation occurs when the local pressure falls below the vapor pressure, causing bubbles to form and collapse, which in turn cause noise, vibration, damage to the propeller, and a significant reduction in thrust provided by the propeller. While some small amount of cavitation is acceptable, the propeller must be designed to perform appropriately over the full range of desired speeds. Typically, risk of cavitation is reduced with increased blade area.

Burrill (1943) developed a criteria for predicting cavitation and revised it in (Burrill and Emerson 1963). He presented the likelihood of cavitation based on a cavitation number and thrust coefficient; the well-known Burrill diagram is used in the early stages of propeller design to avoid cavitation.

Burrill recommended a limit of 5% back cavitation for merchant ship propellers; however, numerous more recent studies of cavitation indicate a higher back cavitation limit is more appropriate; see, for example, (Gawn and Burrill 1957; Black 2007). The American Bureau of Shipping (2018) guidance states that modern merchant ship propellers are designed with airfoil blade sections, making the 10% back cavitation line more appropriate.

Due to these recommendations, ship speed is limited to the speed that corresponds with 10% back cavitation. If this limit falls below the design speed, blade area is increased until the cavitation criteria is met. The user may input a maximum speed, different from the design speed, which the program will ensure is met without significant cavitation through appropriate selection of AE/AO.

Propulsion Power

Having determined the resistance of the ship and the performance of the propeller, the power required to propel the ship through the water is determined. Effective power, P_e, is the power required to overcome the resistance of the ship.

$$P_e = R_T V. \tag{16}$$

Brake power, P_b, is the power that must be produced by the engine and incorporates the effects of propeller open-water efficiency, η_o, hull efficiency, η_h, relative rotative efficiency, η_r, and shaft efficiency, η_s.

$$P_b = \frac{P_e}{\eta_o \eta_h \eta_r \eta_s} \tag{17}$$

Propeller open-water efficiency, η_o, is determined from the propeller estimation process described earlier.

Hull efficiency, η_h, is

$$\eta_h = \frac{1-w}{1-t}, \tag{18}$$

where w is the Taylor wake fraction and t is the thrust deduction factor described below.

The Taylor Wake Fraction, w, accounts for differences in the propeller inflow between the propeller in open water and the propeller behind the hull; w depends on the shape

of the hull and the propeller location and size. Wake fraction is calculated using estimates by Holtrop and Mennen documented in Birk (2019), with separate estimates for a single-screw vessel and a twin-screw vessel.

Wake fraction is normally in the range of 0.2 to 0.45, with large block coefficient ships having relatively large wake fractions. The wake fraction is limited to the range of 0.1 to 0.5.

Per Molland et al. (2017), wake fractions in ballast tend to be 5-15% higher than wake fraction in the loaded condition, resulting in a larger hull efficiency. The revised wake fraction at ballast, w_B, can be determined as (Molland et al. 2017)

$$\frac{(1-w_B)}{(1-w)} = 1 + \left[\frac{T_B}{T} - 1\right](0.2882 + 0.1054\Theta) \qquad (19)$$

where $\Theta = (100 \cdot \text{ trim by bow})/L_{bp}$ is the trim angle. Trim by the bow is measured in meters and will typically be a negative number at ballast.

The Thrust Deduction Factor, t, is also estimated using equations from Holtrop and Mennen (Birk 2019). In general, t is a small positive number somewhere around 0.2. The thrust deduction factor is limited to the range of 0.1 to 0.25.

The thrust deduction factor at ballast, t_B, can be determined using (Molland et al. 2017)

$$\frac{(1-t_B)}{(1-t)} = 1 + \left[\frac{T_B}{T} - 1\right](0.4322 + 0.4880C_b). \qquad (20)$$

Relative Rotative Efficiency, η_r, accounts for differences in performance of the propeller behind the hull other than those dealt with by the wake fraction and the thrust deduction, and is generally near unity; typical values range from 0.96 to 1.04. η_r is estimated using Holtrop and Mennen's recommendation referenced in Birk (2019). Values are limited to a range of 0.95 to 1.05.

Shaft efficiency, η_s, is a scalar value provided by the user. If not provided, η_s is assumed to be 0.99. The shaft efficiency accounts for losses along the shaft due to bearings and other frictional losses.

Examples. Figure 3 shows brake power versus speed for two example ships, along with sea trial data for comparison. Discussion of these results along with numerical comparisons of sea trial data to calculations are provided in the examples section later in the article.

ENGINE CALCULATIONS

All power generated by the engine is assumed to be used for propulsion and no reduction gear is employed; thus, the rotation rate of the engine is equal to the rotation rate of the propeller and the load on the engine is equal to the load on the propeller, increased by the relevant efficiencies.

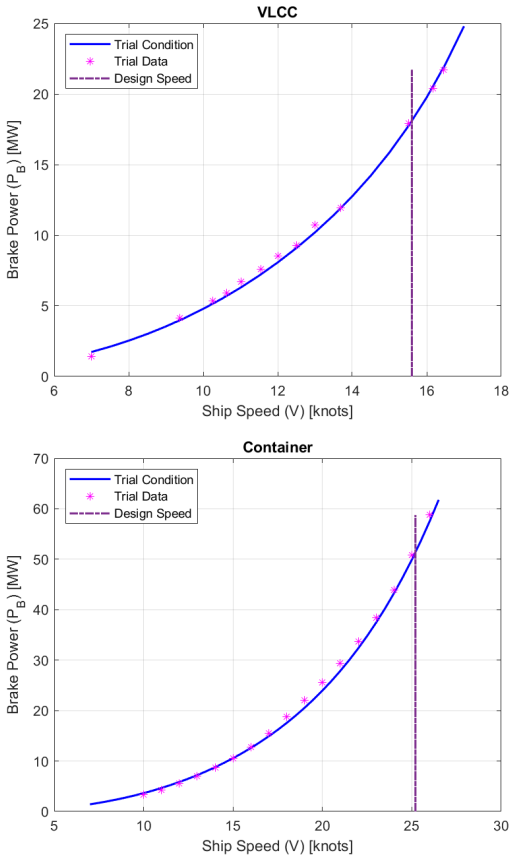

Fig. 3. Brake power as a function of ship speed for a sample VLCC (top) and container ship (bottom).

Each diesel engine has a characteristic layout diagram defined by four points, $L1$, $L2$, $L3$ and $L4$; Fig. 4 shows a representative engine load diagram in light blue. The $L1$ point is the engine's nominal maximum continuous rating (MCR), which is the rated sustained maximum power produced by the engine at the rated sustained maximum rotation rate; these maximum power and rotation rate values can be exceeded by the engine, but only for a short period of time. The line from $L1$ to $L3$ on a log-log plot is a line of constant mean effective pressure (MEP) at the maximum rated MEP for the engine. Lines of constant MEP are parallel to the $L1 - L3$ line.

The ship operational design point is the power and rotation rate required to achieve design speed at a selected design sea state including an engine margin, em, and a propeller margin, pm; this operational design point is termed the specified maximum continuous rating (SMCR). Brake power at SMCR is defined as

$$Pb_{SMCR} = Pb_{hrDes}(1 + em) \qquad (21)$$

where Pb_{hrDes} is the brake power for heavy running at design speed and em is the engine margin, typically 10%. The corresponding engine speed, N_{SMCR}, is the value of the engine speed curve at the SMCR power, N_{hrDes}, decreased by

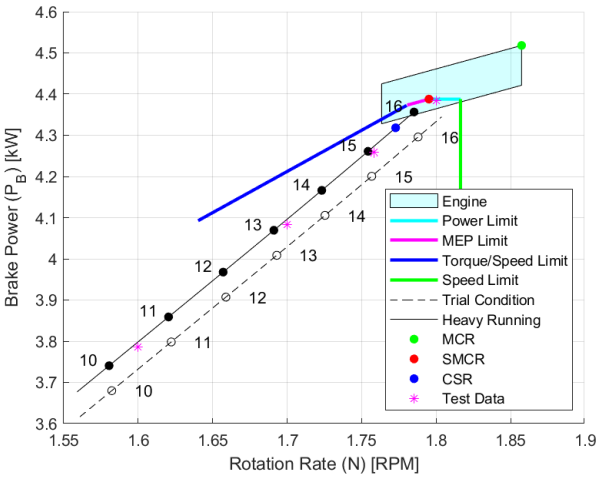

Fig. 4. Engine load diagram and operating limits for an engine installed in a ship. This diagram is for an example VLCC; trial data is denoted.

a propeller margin, pm, typically 5%, such that

$$N_{SMCR} = N_{hrDes}(1 - pm). \tag{22}$$

The SMCR point, defined by the power, Pb_{SMCR}, and the rotation rate, N_{SMCR}, must fall within the engine layout diagram.

To clarify the difference between MCR and SMCR, the MCR is the maximum rated power and speed combination that can be produced by the engine; the SMCR is the maximum rated power and speed combination that can be produced by the engine *as installed in the ship* and includes such impacts as coupling with the propeller and tuning for the application.

The entire operating curve of the engine at all planned speeds and sea states must fall within an area defined by speed, power, mean effective pressure, and torque limits of the engine as installed. An example plot is shown in Fig. 4; note that the trial condition and heavy running propeller curves (solid and dashed black lines respectively) are within the designated limits of the engine as installed (green, cyan, magenta and blue solid lines). Details for calculation of the limiting curves may be found in (MAN Diesel & Turbo 2011).

Engine Performance

Specific fuel oil consumption (SFOC) for an engine varies with mean effective pressure and engine load. The SFOC at 100% engine load is determined by calculating the MEP at SMCR as a percentage of maximum MEP, then using the change in SFOC with MEP to determine SFOC at SMCR. The change in SFOC with MEP is provided in the engine data input.

The SMCR data point is then used to determine SFOC as a function of engine load. Change in SFOC with engine load may be provided as an input to the code in the engine data file. If unavailable, generic values are used as an estimate.

Combining the SFOC versus engine load data with the speed/power curve data determined earlier allows us to determine fuel oil consumption (FOC) in tons per day as a function of speed for an engine tuned to the SMCR at high load.

$$FOC = SFOC \cdot P_b \tag{23}$$

The engine is typically tuned so that peak fuel efficiency occurs between 70 and 80% engine load; this point is termed the continuous service rating (CSR).

PERFORMANCE IMPROVEMENTS

Engine Modifications

Both Wärtsilä and MAN B&W offer several tuning options for their diesel engines which reduce specific fuel oil consumption at certain engine loads, usually at the expense of greater specific fuel oil consumption at other loads. Carbon production is directly and linearly correlated with fuel consumption; however, NOx production is correlated with temperature and thus can increase with improved fuel consumption. These competing tendencies must be balanced to meet regulatory requirements.

Changes to the SFOC can be accomplished through various engine tuning methods such as exhaust gas bypass, variable turbine area, electronic control tuning and turbocharger cut-out, each of which can be tuned for partial load (50-85% of SMCR) or low load (25-70% of SMCR). Changes to the SFOC for each tuning method can be applied to the SFOC values determined previously. These methods will typically reduce SFOC at lower engine load ranges while increasing SFOC at higher engine loads. Methods cannot be combined for further fuel consumption improvements.

The manuals pertinent to each engine provided by the manufacturer generally provide the change in specific fuel consumption with engine load for applicable engine modifications. If the data pertinent to a specific engine is not known, a rough approximation can be determined using generic data provided by the engine manufacturers. Figure 5 provides an example change in engine SFOC with various tuning methods compared to generic SMCR tuning for MAN engines (MAN Energy Solutions 2020); these values are the default used by the program if specific data pertinent to the selected engine are not available for each of the methods described below. Similar data are available for Wärtsilä engines.

Delta or Electronic Control Tuning (ECT) is the adjustment of exhaust valve and injection timing using the electronic controls of the engine to optimize performance at a lower engine load. This tuning method can be applied to any engine with electronic controls (as opposed to camshaft-controlled engines), and does not require any additional equipment or modifications to engine components including turbochargers.

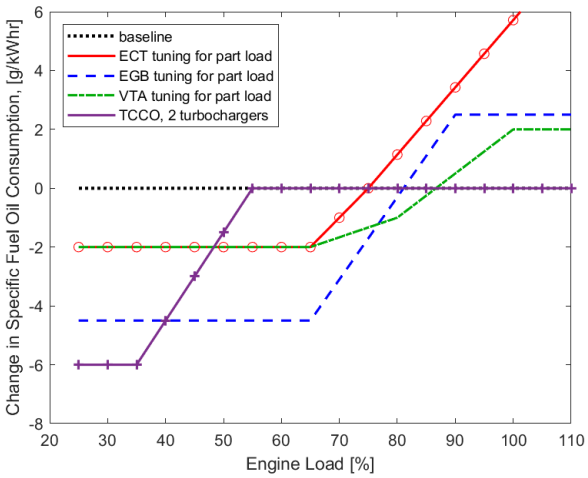

Fig. 5. Change in Specific Fuel Oil Consumption (SFOC) as a function of Engine Load for various tuning technologies (MAN Energy Solutions 2020).

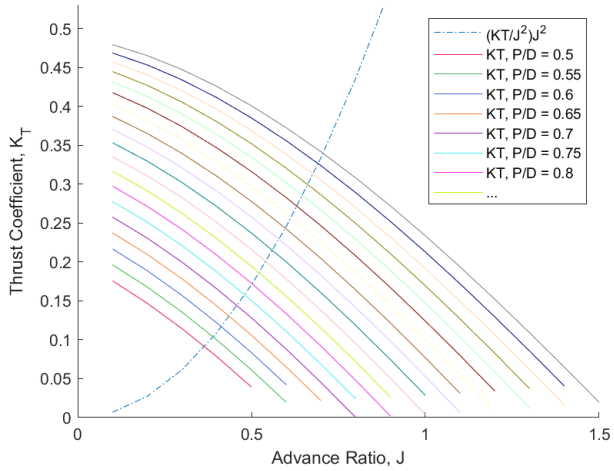

Fig. 6. Intersection of ship performance line, $(K_T/J^2)J^2$, with various propeller performance lines, K_T, for propellers at various P/D ratios.

Variable Turbine Area (VTA) regulates the exhaust gas pressure in order to precisely match the amount of air to the quantity of injected fuel at all points in an engine's load and speed range. The result is reduced specific fuel consumption, reduced emissions of hydrocarbons and carbon dioxide, and improved engine response. VTA requires the replacement of the fixed-vane nozzle rings in standard turbochargers with a nozzle ring equipped with adjustable vanes; altering the pitch of the vanes adjusts the air flow.

Bypass or Exhaust Gas Bypass (EGB) allows the use of smaller turbochargers which have higher efficiencies at lower engine loads. To prevent over-speeding of the turbocharger at high engine loads, an exhaust gas bypass is installed which routes some exhaust gas around the turbocharger at high engine loads. This has the added advantage of increasing exhaust gas temperatures at high loads. EGB requires the installation of an exhaust gas bypass system and, possibly, replacement of the turbochargers.

Turbocharger Cut-Out (TCCO) involves the blanking of one or more turbochargers at low engine loads, either manually or automatically, to improve efficiency at low loads. Savings depend on the general set up of the engine and the number of turbochargers applied. This method requires installation of a blanking device and is applicable to any engine with multiple turbochargers.

Propeller Optimization

The propeller optimization code described in this section is employed when the propeller specifications are not provided in the input data or when a new propeller design is desired. The necessary parameters for propeller design using the Wageningen series are number of blades, diameter, pitch-to-diameter ratio (P/D), expanded area ratio (AE/AO) and design speed. If desired, a maximum speed, greater than design speed, may be entered to ensure cavitation-free operation above the design speed.

Using the number of blades and diameter input by the user, an expanded area ratio is selected using equation Eq. 13, then K_T, K_Q and open water efficiency are calculated for a range of pitch to diameter ratios (P/D) using the Wageningen equations, presenting a family of appropriate propeller curves. The propeller operating point at design speed is determined for each P/D ratio using the J determined by the intersection of $(K_T/J^2)J^2$ for the ship and K_T for the propeller as shown in Fig. 6, following the procedure described earlier.

This matrix of P/D values is carried through the engine efficiency calculation, at which point the optimum P/D, that which produces the lowest fuel consumption at design speed when operated in conjunction with the engine, is selected. Note that the propeller with the highest open water propeller efficiency is not necessarily the most efficient overall choice for a propeller design, because the resulting propeller operating speed may force the engine into a less efficient operating point; therefore, the propeller that results in the best fuel oil consumption is selected.

An example is shown in Fig. 7. The engine brake power/speed point for a range of pitch-to-diameter ratios is plotted against the engine layout diagram. Only those P/D ratios that fall within the diagram are considered for use; of those, the one selected is the P/D ratio that provides the lowest specific fuel oil consumption. Note that in this example, this is not the one with the highest propeller efficiency.

It is possible that the SMCR point does not fall within the engine layout diagram. The can happen if, for example, reducing design speed or installing an energy saving device causes the brake power at design speed to fall below the engine layout diagram for the originally installed engine. In

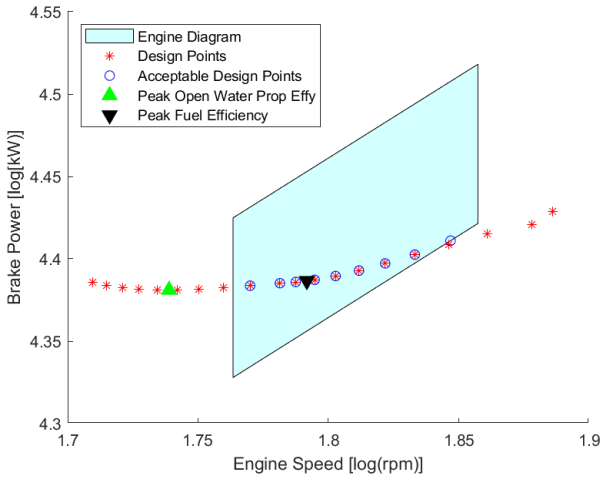

Fig. 7. Optimum propeller design selection.

these instances, the propeller curve is projected until it intersects the engine layout diagram and that intersection point is chosen as the SMCR; in such cases, the design speed will occur at an engine power level other than 100%.

Bulbous Bow Removal

A properly designed bulbous bow reduces propulsion power at and around the designed operating speed of the ship. When a ship is operated at a speed significantly different from the speed for which the bulb was designed, the bulb can have an adverse effect on the resistance of the ship, increasing propulsion power and, thus, fuel consumption. The positive impact of bulbous bows occurs over a fairly narrow range of ship speeds, so bulbs are usually employed in ships that operate at clearly defined speeds for much of their time. If a ship is operated consistently off-design, e.g. due to a new operational profile, it may be cost effective to modify the bulb's shape or to remove the bulb entirely.

Recalling Eq. 3, the only characteristics of the bulb that are used by Holtrop and Mennen to calculate the impact of the bulb on the ship performance are the area and centroid of the transverse cross-section of the bulb at the forward perpendicular; this is a small set of data to capture a vast array of possible performance impacts from differently shaped bulbous bows. Further, the only characteristic of the bulb that is used by Hollenbach is the length of the bulb forward of the forward perpendicular, which is an even smaller set of data. Thus, either estimate is merely a rough approximation of the impact of the bulb on the performance of the ship. *Since this approximation is so rough, any indication from these calculations that bulb removal may be beneficial is merely a recommendation for further study with more detailed analysis of the specific bulb installed in the ship, most likely using computational fluid dynamics and/or model testing.*

Ship Properties with Bulb Removed. Removing the bulbous bow reduces the volume, displacement and wetted surface area of the hull, and thus has a small impact on the *lcb* location and the block coefficient. The following is a description of the process for calculating the impact of bulb removal.

It is strongly preferred that the bulb surface area and volume be entered by the user. If not entered, it is assumed that the bulb is approximately a half-ellipsoid, so the bulb volume, ∇_b is calculated as

$$\nabla_b = \frac{2}{3} A_{bt} L_b \tag{24}$$

where A_{bt} is the transverse cross-sectional area of the bulb at the forward perpendicular and L_b is the bulb length forward of the forward perpendicular. The bulb surface area is approximated using

$$A_b = 2\pi \left(\frac{(\pi A_{bt})^{1.6} + 2(L_b \sqrt{\pi A_{bt}})^{1.6}}{3} \right)^{(1/1.6)} \tag{25}$$

These values are used to calculate a new wetted surface area, volume, displacement, and longitudinal center of buoyancy of the ship without the bulb.

The change in draft is negligible since the buoyancy of the bulb relative to the buoyancy of the entire ship is small, and, further, this small loss in buoyancy is partially offset by a reduction in weight due to steel that is removed. For example, a sample container ship bulb displaces 330 tonnes of seawater; with a 120 tonnes/cm immersion at design draft, removal of the bulb results in less than a 3 cm change in draft; accounting for the change in ship weight due to removal of the steel in the bulb would result in an even smaller change in draft.

Bulb removal changes neither L_{bp} nor B, and change to T is negligible, so there is a very small change in block coefficient, C_b.

Bulb Removal using Holtrop and Mennen. After recalculating the above properties of the now bulb-less ship, the reduction to wave resistance in Holtrop and Mennen due to the presence of a bulbous bow is eliminated by setting the A_{bt} and h_b values to zero. At this point, the resistance, propeller and engine calculations are run using the new bulb-less ship properties to determine the power and fuel required for an equivalent ship with the bulb removed.

Bulb Removal using Hollenbach. In Hollenbach's calculations, the impact of the bulbous bow is accounted for solely by increasing the ship length to include the length of the bulb. In order to measure the impact of eliminating the bulbous bow, one does not get reasonable results by merely decreasing the length of the ship by the amount of bulb removed and decreasing the surface area by the surface area of the removed portion of the bulb, because the resulting calculation indicates an increased resistance over the full range of ship speeds, rather than the expected profile in which resistance is lower at low speeds but higher at high speeds in

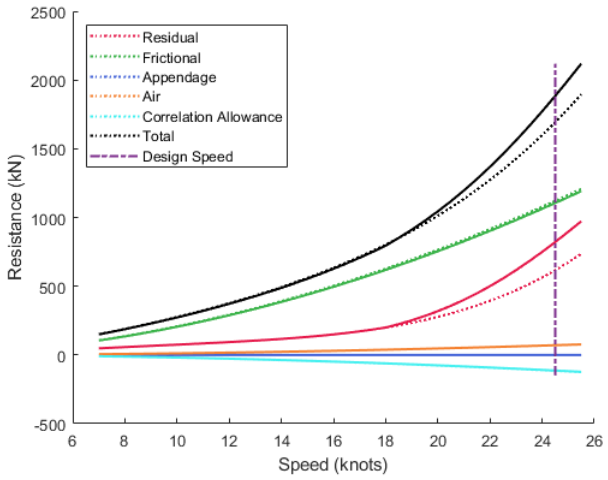

Fig. 8. Resistance calculations using Hollenbach. Ship with bulb shown in dotted lines; ship without bulb shown in solid lines.

the bulb-less ship as compared to the equivalent ship with a bulb.

To estimate the impact of the bulb, the formulation proposed by Kracht (1978), who employs a residual power reduction coefficient, $\Delta C_{P\nabla R}$, is used to capture the change in residual resistance for a ship with and without a bulb,

$$\Delta C_{P\nabla R} = 1.0 - C_{Rwith}/C_{Rwithout}, \tag{26}$$

where C_{Rwith} and $C_{Rwithout}$ are residual resistance coefficients of equivalent ships with and without a bulb.

It is assumed, for any ship using the Hollenbach formulation, that the maximum $\Delta C_{P\nabla R}$ is equal to 0.25 and occurs at the design speed. Further, the $\Delta C_{P\nabla R}$ is assumed to be parabolic with a minimum value of zero occurring at the point in which residual resistance becomes nonlinear.

To apply this assumption, Hollenbach's residual resistance for the ship with the bulb is calculated. Then, the inflection speed at which the residual resistance changes from linear to higher order is found and a correction is applied such that $\Delta C_{P\nabla R} = 0.0$ at the inflection speed and changes in a parabolic form to a maximum of $\Delta C_{P\nabla R} = 0.25$ at design speed, then decreases above design speed, again parabolically. $\Delta C_{P\nabla R}$ is constrained to always be non-negative. The remainder of the resistance elements are calculated using updated values for the bulb-less ship. Figure 8 shows a calculation for a ship with a bulb shown in dotted lines and without the bulb shown in solid lines. Note that the residual resistance without the bulb is higher than the residual resistance with the bulb at higher speeds. The frictional resistance is lower for the ship without the bulb through the full speed range. The total resistance is slightly lower at low speed and higher at high speeds.

Energy Saving Devices

A variety of energy saving devices can be implemented which, in general, have the effect of modifying flow into or out of the propeller in a manner that improves efficiency through some range of speeds. Examples include propeller boss cap fins, ducted propellers, pre-swirl stators and asymmetric rudders or hulls, among others.

One potential fuel-saving technology is the Mewis duct (Guiard et al. 2013), which is advertised to achieve a fuel savings in the neighborhood of 5 to 7 percent, depending on the thrust coefficient, C_{th}, of the original vessel.

$$C_{th} = \frac{T_o}{\frac{1}{2}\rho\pi\frac{D^2}{4}(V_a)^2}, \tag{27}$$

where T_o is thrust and V_a is the water speed at the propeller.

Since the ship data provided to this program are not particularly detailed, it is not possible to accomplish a full CFD-scale simulation of the Mewis duct; further, the information necessary to properly modify the wake fraction, w, thrust deduction factor, t, and relative rotative efficiency, η_r, for a ship with a Mewis duct installed is not available. Therefore, the process used to estimate the impact of the Mewis duct is to calculate the ship's thrust coefficient using the standard thrust value, then use the plot shown in Fig. 9 to determine a power reduction that is applied to the brake power. Guiard et al. (2013) also report a slight increase in propeller rotation rate on the order of 1%, so the propeller rotation rate is increased by 1% as well. These modifications to power and rotation rate are applied before the engine SFOC calculations.

Per Mewis and Guiard (2011), impact of the Mewis Duct is even greater in ballast than in loaded condition. For example, 35 model tests with and without a Mewis Duct show an average of a 5.7% power reduction at design draft, and a 7.3% power reduction at ballast draft. This increased impact at ballast is not currently included.

DATA ESTIMATES AND CALCULATIONS

The program described herein requires a bare minimum of essential data in order to estimate ship performance and potential energy savings; however, the predictions improve greatly with additional data provided. This section describes the methodologies for estimating any missing input data and cites the sources for the estimates.

Displacement

If displacement at design draft is not entered, it can be estimated from deadweight, DWT, as (MAN Diesel & Turbo 2011)

$$\Delta = k_\Delta DWT \tag{28}$$

where $k_\Delta = 1.17$ for tankers and bulkers, and $k_\Delta = 1.33$ for container ships.

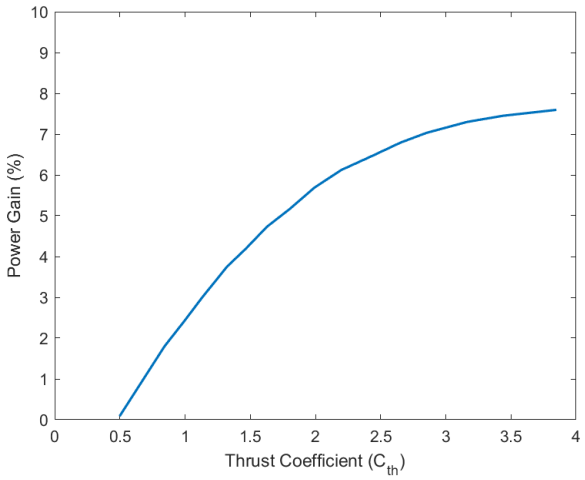

Fig. 9. Power savings claimed by the Mewis duct, as a function of thrust coefficient, C_{th}, per (Guiard et al. 2013).

If displacement at ballast condition, Δ_B, is not provided, then it is estimated from displacement at design draft using

$$\Delta_B = \Delta - \rho C_{wp} B L_{wl} (T - T_B) \tag{29}$$

where T is mean draft at design draft, T_B is mean draft at ballast, and C_{wp} is the waterplane coefficient. A lower limit is placed on this calculation such that ballast displacement must be at least 10% of displacement at design draft.

Length

Length at the waterline, L_{wl}, and length between perpendiculars, L_{bp}, are both required. If neither is provided, then L_{wl} is estimated as (MAN Diesel & Turbo 2011)

$$L_{wl} = 0.956 L_{oa} \tag{30}$$

where L_{oa} is length overall.

The difference between L_{wl} and L_{bp} is the distance from the aft perpendicular to the aftmost point of the wet hull, d_{ap},

$$L_{wl} = L_{bp} + d_{ap}. \tag{31}$$

If L_{wl} and L_{bp} are not provided and d_{ap} is not available, the relationship between L_{wl} and L_{bp} is be estimated as

$$L_{wl} = k_{ll} L_{bp} \tag{32}$$

where $k_{ll} = 1.01$ for tankers and bulkers and $k_{ll} = 1.02$ for container ships (Kristensen and Lützen 2012).

Block Coefficient

Block coefficient, C_b, is defined as the volumetric displacement of the ship divided by the volume of the bounding box around the wetted hull

$$C_b = \frac{\nabla}{L_{wl} B T}. \tag{33}$$

Note that the volumetric displacement and mean draft must correspond with one another; both are expected to be at design draft.

Per (MAN Diesel & Turbo 2011), block coefficients for tankers and bulkers range 0.80 - 0.85, and for container ships range from 0.50 - 0.70. C_b is assumed to be 0.8 for tankers and bulkers, and 0.6 for container ships if the appropriate dimensions are not provided by the user. If beam, B, is not provided, beam is calculated from the block coefficient, length and draft using Eq. 33.

Midship Section Coefficient

The midship section coefficient, C_x, is defined as the midship section area, A_x, divided by the bounding box of that area, $C_x = A_x/BT$. If C_x is not provided by the user, then it is estimated using (Birk 2019)

$$C_x = \frac{1}{1 + (1 - C_b)^{3.5}}. \tag{34}$$

Waterplane Area Coefficient

The waterplane area coefficient, C_{wp}, is defined as the area of the waterplane divided by the bounding box of that area, $C_{wp} = A_{wp}/L_{wl}B$. If C_{wp} is not provided, it is estimated using (Birk 2019)

$$C_{wp} = k_{wp1}(C_p + k_{wp2}); \tag{35}$$

where $k_{wp1} = 0.763$ and $k_{wp2} = 0.34$ for tankers and bulkers with $0.56 < C_p < 0.87$, and $k_{wp1} = 3.226$ and $k_{wp2} = -0.36$ for container ships with $0.57 < C_p < 0.62$; otherwise, C_{wp} is assumed to equal 0.907.

Wetted Surface Area

If the wetted surface area, A_{ws}, is not provided, Mumford's formula as modified by Kristensen and Lützen (2012) is used:

$$A_{ws} = k_{ws}(\frac{\nabla}{T} + 1.9 L_{wl} T) \tag{36}$$

where $k_{ws} = 0.990$ for tankers and bulkers and $k_{ws} = 0.995$ for container ships. This surface area, A_{ws}, describes the bare hull only.

If not provided, the wetted surface area of appendages is estimated to be

$$A_{app} = 0.7T + 0.015 L_{wl}. \tag{37}$$

If the wetted surface area in ballast, A_{wsB}, is not provided, then it is estimated from wetted surface at design draft using

$$A_{wsB} = A_{ws} - k_b (T - T_B)(L_{wl} - B) \tag{38}$$

where T is mean draft at design draft, T_B is mean draft at ballast, and $k_b = 2.0$ for tankers and bulkers or $k_b = 2.4$ for container ships (Birk 2019).

Longitudinal Center of Buoyancy

If the distance of the longitudinal center of buoyancy from the aft perpendicular, lcb_{ap}, is not provided, Guldhammer and Harvald's estimate of the best possible lcb location is used, given as a percentage of waterline length forward of the mean of the waterline (Guldhammer and Harvald 1974)

$$lcb = 9.4 - 43.8Fr_{des} \tag{39}$$

where Fr_{des} is the Froude number at design speed.

Transverse Area Exposed to Wind

The transverse area exposed to wind, A_{exp}, is the transverse cross-sectional area of the hull and superstructure, including cargo, above the design waterline. This area is in a plane orthogonal to forward motion. If A_{exp} is not provided, it is estimated to be

$$A_{exp} = BT. \tag{40}$$

If area exposed to wind at ballast, A_{expB}, is not provided, it is assumed that the exposed area at design draft is increased by the change in trim forward multiplied by the beam:

$$A_{expB} = A_{exp} + (T_{fB} - T_f)B \tag{41}$$

where T_{fB} is trim forward at ballast.

Propeller Diameter

It is strongly encouraged that the propeller diameter, D, be provided by the user. If unavailable, propeller diameter is estimated using (Kristensen and Lützen 2012)

$$D = k_{d1}T + k_{d2} \tag{42}$$

where $k_{d1} = 0.395$ and $k_{d2} = 1.30$ for tankers and bulkers, or $k_{d1} = 0.623$ and $k_{d2} = -0.16$ for container ships.

Propeller Hub Depth

If not provided, the depth of the center of the propeller hub, h, is estimated as

$$h = T - D/2. \tag{43}$$

Expanded Area Ratio

As stated earlier, the propeller expanded area ratio, AE/AO, is estimated based on cavitation considerations if it is not provided by the user. The initial rough estimation uses an equation proposed by Keller and referenced in Birk (2019):

$$\frac{AE}{AO} = \frac{(1.3 + 0.3Z)Th}{(p_0 - p_v)D^2} + K \tag{44}$$

where Th is thrust at design speed, p_0 is the hydrostatic pressure at the centroid of the propeller hub, p_v is the saturation pressure of the water which equals 2,291 Pa at 20^{o}C, D is the propeller diameter, and the constant K is

$K = 0.2$ for single-screw vessels
$K = 0.1$ for slow twin-screw vessels
$K = 0.0$ for fast twin-screw vessels.

For the purposes of this code, slow is defined as 20 knots or less and fast is greater than 20 knots. Thrust, Th, is calculated as

$$Th = \frac{R_{hrDes}}{(1-t)} \tag{45}$$

where R_{hrDes} is the heavy-running resistance at design speed and t is the thrust deduction factor. Hydrostatic pressure, p_0, is

$$p_0 = P_{atm} + \rho gh \tag{46}$$

where ρ is seawater density, g is the gravitational constant, and h is the draft of the centroid of the propeller hub. Note that the full propeller calculation includes a further check on cavitation and, if cavitation levels are exceeded, AE/AO is increased until cavitation requirements are met.

EXAMPLES

In this section examples of a very large crude carrier (VLCC) and a container ship are provided. Where available, data from the actual ship test data or operational data is compared to the calculations. Table 2 shows input data for the two example ships.

Very Large Crude Carrier (VLCC)

The first example ship is a VLCC. Beginning with the resistance calculation using Holtrop and Mennen, results are presented in Fig. 1. The majority of the speed range is in the regime dominated by frictional resistance.

Since the pitch/diameter ratio (P/D) was not provided, the program calculated the P/D to be 0.76 to achieve the minimum specific fuel oil consumption as shown in Fig. 7. Cavitation limits are well above design speed and therefore acceptable.

The resultant brake power for trial condition is presented in Fig. 3 along with sea trial and log data corresponding to trial condition. The difference between the log data and the estimate ranges from 0.3 to 6.2 percent, with the majority being within five percent; see Table 3.

Figure 4 presents the engine load diagram with calculated propeller curves and trial data denoted. The test data is appropriately bracketed by the propeller curves for trial and heavy running conditions.

Specific fuel oil consumption for the engine tuned to SMCR and for various engine modifications is plotted in Fig. 10. From the test data plotted in the figure, it is evident that the engine is tuned for lower engine loads, most likely using the ECT low-load modification. Change in fuel oil consumption from the baseline engine tuned to SMCR is also shown in Fig. 10.

Container Ship

The second example is a container ship. Container ships typically operate at higher speeds than tankers and thus operate in a regime that includes wave resistance; this can be

Table 2. Input data for example vessels

Ship Name	VLCC	Container
hullform data		
ship type	tanker	container
bulbous bow	no	yes
energy-saving device	no	no
design speed [kt]	15.6	25.2
LBP [m]	324	334
LWL [m]	330	333
beam [m]	60	45.6
design draft [m]	20.5	13
displ at Design Draft [kmt]	333	128
LCB to AP [m]	173	161
AP to aft wet hull [m]	7	–
wetted surface area [m^2]	28,023	17,735
transv area above water [m^2]	1,227	1,830
ballast draft forward [m]	8	–
ballast draft aft [m]	11	–
midship section coefficient	0.999	0.985
water-plane coefficient	0.907	0.803
bulb length from FP [m]	–	12
transv sect area of bulb [m^2]	–	38
vert centroid of bulb area [m]	–	7.6
rudder surface area [m^2]	270	–
engine data		
engine make	MAN	Wärtsilä
engine model	G80MEC9.2	RTA96C
engine control	Electronic	Electronic
number of cylinders	7	12
propeller data		
number of props	1	1
diameter [m]	10.6	8.8
propeller ht above BL [m]	15	–
number blades	4	6
expanded area ratio	0.4	0.95
pitch/diameter ratio	–	0.9895
margins		
engine margin	0.2	0.1
sea margin	0.15	0.15
shaft efficiency	0.99	0.99

Table 3. Comparison of calculated values to ship measurement data from sea trials and operational logs for the example VLCC brake power in MW at trial condition, as shown in Fig. 3.

Speed [kt]	Calculated [MW]	Data [MW]	Difference [%]
9.4	3.987	4.157	-4.1
10.3	5.135	5.346	-4.0
10.6	5.697	5.904	-3.5
11.0	6.300	6.717	-6.2
11.5	7.211	7.576	-4.8
12.0	8.073	8.532	-5.4
12.5	9.090	9.282	-2.1
13.0	10.201	10.713	-4.8
13.7	11.909	11.950	-0.3
15.5	17.716	17.900	-1.0
16.2	20.545	20.402	0.7
16.4	21.851	21.715	0.6

seen in Fig. 1, where wave resistance begins to become significant at about 20 knots. The estimated resistance has quite good correlation with the model test data in this figure, ranging from 0.1 to 6.7 percent difference at any point, even extending into the wave-dominated regime, as shown in Table 5. The close correlation is especially notable in view of the uncertainty involved in estimating the impact of the bulbous bow.

Another area of interest in this example is the propeller curves. Container ships tend to have more complex propellers with greater skew and rake than a tanker propeller, so there was some concern that using the Wageningen B-Series as an estimate of propeller performance might be a source of error; however, good correlation is found between the estimated propeller and propeller test data provided by the ship owner. In Fig. 2, the calculated propeller data is shown using solid lines and the corresponding actual propeller data is plotted using symbols. In the operational regime for this vessel, J is between 0.64 and 0.685, and the calculated propeller efficiencies in this range are within 2% of the actual values, as shown in Table 4.

This ship employs a Wärtsilä engine, so a different array of tuning technologies are available than for the MAN B&W engines used by the previous example vessel. The impacts of these technologies on fuel consumption for this example ship are shown in Fig. 11.

Modifications of the container ship were run to estimate changes for bulbous bow removal, new designed propeller for lower speed operations, installation of an energy-saving device (ESD), and a combination of ESD and new propeller. Results are shown in Fig. 11.

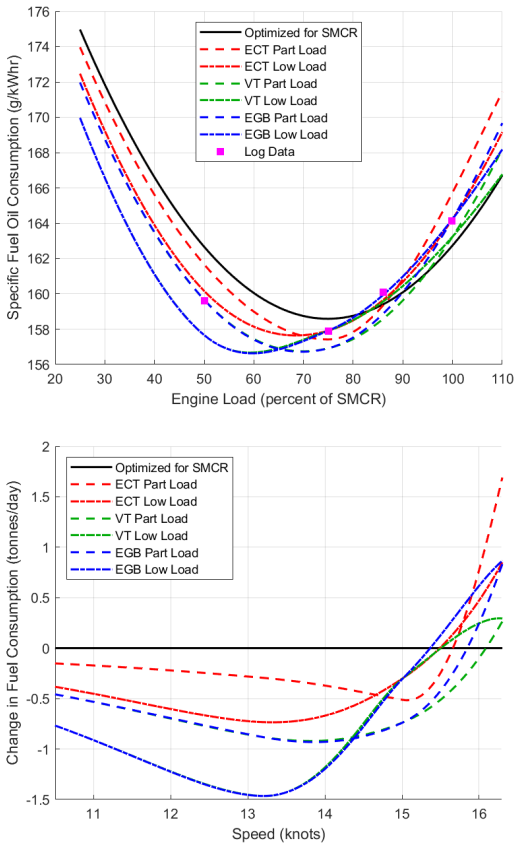

Fig. 10. Specific fuel oil consumption for various engine modifications for the example VLCC along with engine test data (top), and change in fuel oil consumption in tonnes/day for various engine modifications (bottom).

Example Conclusions

Example calculations have been presented for a container ship and a VLCC. The comparison of each ship to operational or test data shows exceptional correlation between the program's calculations and actual ship data, especially given the simplicity of the inputs provided.

VALIDATION

The code has been tested for a large set of ships of various types and a wide variety of sizes, and has been found to closely align with model test data and sea trial data throughout.

The performance characteristics of 23 ships were modeled: 13 tankers, 7 bulkers, and 3 container ships ranging in size from 37,000 to 318,000 DWT, and in age from one to 20 years. The calculated estimates of brake power in the sea trial condition are compared with brake power measurements from sea trial reports for those ships. The average discrepancy between model and sea trial power for these 23 ships, in the range of speeds at which sea trial measurements are reported, is less than 2.5%. Figure 12 shows the design speed data point for each of these ships plotted against a line depicting perfect correlation.

Table 4. Comparison of log data and estimated data for container ship propeller curves.

Advance Ratio J	0.60	0.65	0.70
K_T Calculated	0.244	0.218	0.191
K_T Data	0.251	0.223	0.196
K_T % Difference	2.7	2.4	2.8
K_Q Calculated	0.408	0.373	0.337
K_Q Data	0.423	0.388	0.353
K_Q % Difference	3.6	3.9	4.6
η_o Calculated	0.572	0.604	0.630
η_o Data	0.565	0.595	0.620
η_o % Difference	1.2	1.5	1.6

This robust testing provides confidence that the procedure is appropriate for the vast bulk of cargo ships operating today.

CONCLUSIONS AND FUTURE WORK

Summary. The goal of this project is to reduce carbon production of the existing cargo shipping fleet by providing an easy-to-use tool that assesses the impact that various fuel-saving methods and technologies have on fuel consumption. The code uses a small set of input data to estimate baseline ship performance and then provides the energy-saving impact of slow steaming, propeller redesign, bulbous bow removal, engine modifications, and energy-saving device installation.

The minimum data required include ship type, length, beam, draft, displacement, design speed, number of propellers, engine layout data, and indication of the presence of a bulbous bow or energy-saving device. The accuracy of resistance estimates can be improved by increasing the amount of data provided to the program including information such as bulbous bow dimensions, longitudinal center of buoyancy, hull shape coefficients, surface areas, and propeller details. If these additional data are not provided, the program estimates input values.

Results are provided in terms of fuel usage and savings for each potential modification and for combinations of modifications. Estimates for both fully-laden and ballast condition are provided.

The code has been applied to a wide variety of ship types including supertankers, product tankers, bulk carriers and container ships of various sizes, and the results were compared to actual measured data for the ships operating at sea, with impressive correlation between the estimates and the measured data. The code described herein has been used by Marsoft, Inc. to forecast the economic impact of ship modifications.

Further description of the code including theoretical background and a user's guide are available in (Chal-

Table 5. Comparison of calculated resistance to test data for container ship total resistance.

Speed [kt]	Calculated [MN]	Data [MN]	Difference [%]
11	0.557	0.528	5.5
12	0.644	0.623	3.4
13	0.737	0.725	1.6
14	0.836	0.835	0.2
15	0.943	0.952	-1.0
16	1.057	1.077	-1.9
17	1.180	1.232	-4.3
18	1.313	1.400	-6.3
19	1.457	1.562	-6.7
20	1.615	1.722	-6.2
21	1.788	1.890	-5.4
22	1.977	2.066	-4.3
23	2.186	2.252	-3.0
24	2.415	2.464	-2.0
25	2.669	2.732	-2.3
26	2.948	3.031	-2.7

fant et al. 2021). The code is available for download at https://seagrant.mit.edu/decarbonization/

Future Work. The code is applicable to direct-drive ships with fixed-pitch propellers and no reduction gear. Possible future expansions that would be relatively simple to implement would be to add capability for reduction gears, controllable-pitch propellers, and electric drive or power-take-off configurations. Additional energy saving devices beyond the Mewis Duct warrant further investigation as well.

There are a number of quite interesting energy-saving methods that are not examined in the current project such as waste-heat recovery, energy storage, air lubrication of the hull, or incorporation of renewable resources such as wind power. These would likely require significant modification to existing ships, but have the potential to provide significant energy savings.

Machine-learning techniques and the use of big data would be useful to parse voyage data for prediction of maintenance and repair needs which can unearth energy-saving methods such as timely hull cleaning with low cost and high impact.

Conclusion. In this research a large variety of ship performance research has been incorporated to produce an extremely useful tool to today's ship owners, allowing the analysis of the existing cargo fleet to determine the best methods for achieving significant carbon reduction goals.

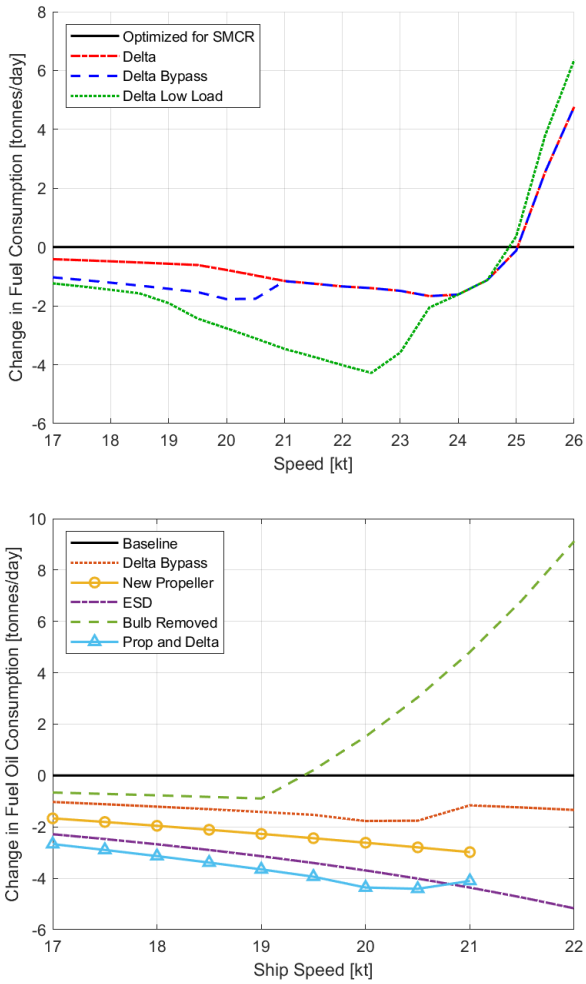

Fig. 11. Change in fuel oil consumption for various engine modifications (top) and other modifications (bottom) for the container ship.

ACKNOWLEDGEMENTS

This material is based upon research funded by the Hightide Foundation in collaboration with Marsoft Inc. Their sponsorship and support is greatly appreciated.

Prof. Pradya Prempraneerach was involved in the beginning of the project but, because of travel restrictions due to the pandemic, was unable to continue the collaboration. His original contributions were extremely valuable.

References

American Bureau of Shipping. 2018. *Guidance Notes on Ship Vibration.* Technical report. February.

Birk, Lothar. 2019. *Fundamentals of Ship Hydrodynamics: Fluid Mechanics, Ship Resistance and Propulsion.* First. Hoboken, NJ, USA: John Wiley & Sons Ltd. ISBN: 9781118855515.

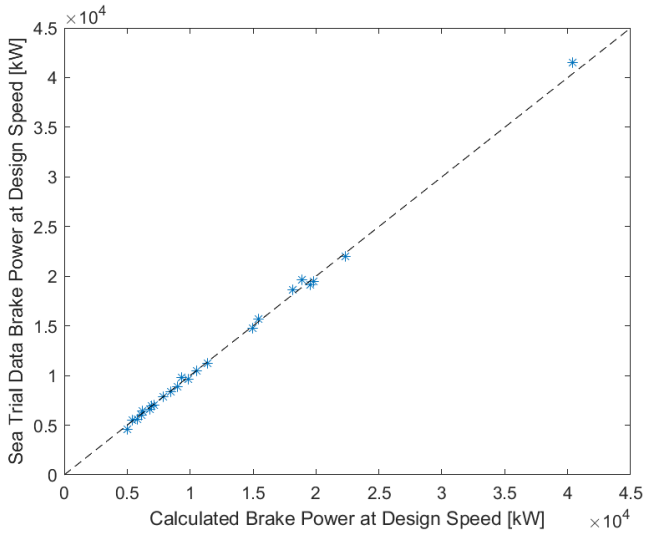

Fig. 12. Comparison of calculated data to sea trial data at design speed. Each star represents a single ship at design speed. The dashed line indicates perfect correlation.

Black, Scott D. 2007. *Thrust Breakdown Characteristics of Conventional Propellers.* Technical report NSWCCD-50-TR-2007/064. Naval Surface Warfare Center Carderock Division, September.

Bonfiglio, Luca, and Dario Boote. 2009. "Progetto di massima di una portacontenitori da 9000 TEU." Master's thesis, Università di Genova.

Buhaug, Ø, JJ Corbett, O Endresen, V Eyring, J Faber, S Hanayama, D Lee, et al. 2009. "Second IMO greenhouse gas study." *International Maritime Organization, London.*

Burrill, L. C. 1943. "Developments in Propeller Design and Manufacture for Merchant Ships." *Transactions, Institute of Marine Engineers* (London) 55.

Burrill, LC, and A Emerson. 1963. "Propeller cavitation: Further tests on 16in. propeller models in the King's College cavitation tunnel." *International Shipbuilding Progress* 10 (104): 119–131.

Chalfant, J. S., L. Bonfiglio, and C. Chryssostomidis. 2021. *Decarbonization of the Cargo Shipping Fleet.* Technical report. MIT Sea Grant Report Number 2019-R/RCM-64-LEV. MIT Sea Grant College Program.

Engineering Toolbox. 2022. "Fuels - Densities and Specific Volumes." Accessed February 23, 2022. https://www.engineeringtoolbox.com/fuels-densities-specific-volumes-d_166.html.

Gawn, R. W., and L. C. Burrill. 1957. "Effect of Cavitation on the Performance of a Series of 16 inch Model Propellers." In *RINA Transactions,* vol. 1957-32. London.

Guiard, Thomas, Steven Leonard, and Friedrich Mewis. 2013. "The Becker Mewis Duct - Challenges in Full-Scale Design and New Developments for Fast Ships." In *Third International Symposium on Marine Propulsors (SMP'13).* Launceston, Tasmania, Australia, May.

Guldhammer, HE, and Sv Aa Harvald. 1974. "Ship Resistance - Effect of form and principal dimensions (revised)." *Danish Technical Press, Copenhagen, Denmark.*

Holtrop, J. 1984. "Statistical re-analysis of resistance and propulsion data." *International Shipbuilding Progress* 31 (363): 272–276.

———. 1988. "A statistical resistance prediction method with a speed dependent form factor." In *Proceedings of SMSSH (Scientific and Methodological Seminar on Ship Hydrodynamics),* 1–7. Varna, Bulgaria, October.

Holtrop, J., and G. G. J. Mennen. 1978. "A statistical power prediction method." *International Shipbuilding Progress* 25 (290): 253–256.

———. 1982. "An approximate power prediction method." *International Shipbuilding Progress* 29 (335): 166–170.

International Maritime Organization. 2020. *Reducing greenhouse gas emissions from ships.* Https://www.imo.org/en/MediaCentre/HotTopics/Pages/Reducing-greenhouse-gas-emissions-from-ships.aspx. Accessed December 11, 2020.

Kracht, Alfred M. 1978. "Design of bulbous bows." *SNAME Transactions* 86 (1): 197–217.

Kristensen, Hans Otto, and Marie Lützen. 2012. "Prediction of resistance and propulsion power of ships." *Clean Shipping Currents* 1 (6): 1–52.

Lewis, E.V., ed. 1988. *Principles of Naval Architecture.* Volume II – Resistance, Propulsion and Vibration. Jersey City, NJ, USA: Society of Naval Architects & Marine Engineers. ISBN: 0-939773-01-5.

MAN Diesel & Turbo. 2011. *Basic Principles of Ship Propulsion.* Technical report. Copenhagen SV, Denmark.

MAN Energy Solutions. 2018. *MAN B&W G80ME-C9.5-TII Project Guide.* Technical report. Https://man-es.com/marine/products/two-stroke-engines/two-stroke-engines-portfolio. Copenhagen SV, Denmark, November.

———. 2020. "Tier II Tuning Methods for Two-Stroke Engines." Accessed September 1, 2020. https://turbocharger.man-es.com/technologies/tuning-methods-comparison.

Mewis, Friedrich, and Thomas Guiard. 2011. "Mewis Duct – New Developments, Solutions and Conclusions." In *Second International Symposium on Marine Propulsors (SMP'11).* Hamburg, Germany, June.

Molland, Anthony F, Stephen R Turnock, and Dominic A Hudson. 2017. *Ship resistance and propulsion.* Cambridge, United Kingdom: Cambridge University Press.

NOAA. 2020. *Ocean Acidification.* Https://www.noaa.gov/education/ resource-collections/ocean-coasts/ocean-acidification.

Tans, Pieter, Ed Dlugokencky, and Ben Miller. 2020. *The Power of Greenhouse Gases.* Https://www.esrl.noaa.gov/gmd/ccgg/ghgpower/, October.

Thoman, R. L., J. Richter-Menge, and M. L. Druckenmiller, eds. 2020. *Arctic Report Card 2020.* National Oceanic & Atmospheric Administration. https://doi.org/10.25923/mn5p-t549.

U.S. Environmental Protection Agency. 2020. *Direct Emissions from Mobile Combustion Source.* Technical report. December.

UNCTAD. 2018. *Review of Maritime Transport 2018.* United Nations Conference on Trade and Development, New York. October.